Mice lacking MAP kinase phosphatase-1 have enhanced MAP kinase activity and resistance to diet-induced obesity

J. Julie Wu,[1,6] Rachel J. Roth,[1] Ethan J. Anderson,[2,5] Eun-Gyoung Hong,[3] Mi-Kyung Lee,[3] Cheol Soo Choi,[3] P. Darrell Neufer,[2,5] Gerald I. Shulman,[3,4] Jason K. Kim,[3,7] and Anton M. Bennett[1,*]

[1] Department of Pharmacology
[2] Department of Cellular and Molecular Physiology
[3] Department of Internal Medicine, Section of Endocrinology and Metabolism
[4] Howard Hughes Medical Institute
Yale University School of Medicine, New Haven, Connecticut 06520
[5] The John B. Pierce Laboratory, New Haven, Connecticut 06520
[6] Present address: National Institutes of Health, Maryland.
[7] Present address: Pennsylvania State University College of Medicine, Pennsylvania.
*Correspondence: anton.bennett@yale.edu

Summary

The mitogen-activated protein kinases (MAPK) play critical roles in the pathogenesis of diabetes and obesity. The MAPKs are inactivated by MAPK phosphatases (MKPs) either in the cytosol or nucleus. Here we show that mice lacking the nuclear-localized MKP, MKP-1 (*mkp-1*$^{-/-}$), have enhanced Erk, p38 MAPK and c-Jun NH_2-terminal kinase (JNK) activities in insulin-responsive tissues as compared with wild-type mice. Although JNK promotes insulin resistance, *mkp-1*$^{-/-}$ mice exhibited unimpaired insulin-mediated signaling and glucose homeostasis. We reconciled these results by demonstrating that in *mkp-1*$^{-/-}$ mice, JNK activity was increased in the nucleus, but not the cytosol. Significantly, *mkp-1*$^{-/-}$ mice are resistant to diet-induced obesity due to enhanced energy expenditure, but succumb to glucose intolerance on a high fat diet. These results suggest that nuclear regulation of the MAPKs by MKP-1 is essential for the management of metabolic homeostasis in a manner that is spatially uncoupled from the cytosolic actions of the MAPKs.

Introduction

Stress-responsive stimuli activate a family of enzymes known as the mitogen-activated protein kinases (MAPKs) (Davis, 2000; Ono and Han, 2000). p38 MAPK and c-Jun NH_2-terminal kinase (JNK) are stress-responsive MAPKs that initiate adaptive events such as gene expression, differentiation, metabolism and apoptosis (Davis, 2000; Ono and Han, 2000). A wealth of information exists about the activators of the MAPKs, the MAPK kinases, and their physiological roles (Brancho et al., 2003; Nishina et al., 1999; Tournier et al., 1999). In contrast, little is known about the in vivo role of the MAPK phosphatases (MKPs) that inactivate the MAPKs by dephosphorylation of the regulatory threonine and tyrosine residues on MAPK (Camps et al., 2000; Keyse, 2000).

Metabolic syndrome is a clinical constellation of symptoms that include obesity, hypertension, insulin resistance, glucose intolerance, nonalcoholic fatty liver disease, and hyperlipidemia (Kopelman, 2000). In many cases, metabolic syndrome is associated with increased inflammatory responses. Elevated production of cytokines (e.g., TNF-α) and free fatty acids are implicated in the etiology of obesity-induced insulin resistance (Bays et al., 2004) which often results in the activation of the MAPKs. Additionally, the MAPKs have been reported to become activated following metabolic stresses such as high-fat feeding, atherogenesis and genetic models of obesity. For instance, JNK activity has been shown to be elevated following a high-fat diet (HFD) and in genetic models of obesity in the liver, skeletal muscle and adipose tissue (Hirosumi et al., 2002). p38 MAPK is hyperactivated in models of diet-induced obesity in skeletal muscle (Leng et al., 2004), liver and heart (Li et al., 2005). Whereas, in genetic models of obesity, Erk activity is elevated in the liver (Gum et al., 2003) and adipose tissue (Bost et al., 2005). The pathophysiological consequence of altered MAPK activity in metabolic syndrome still remains to be fully defined. However, JNK has been proposed to negatively regulate insulin signaling thereby promoting insulin resistance (Hirosumi et al., 2002), whereas p38 MAPK is implicated in the positive regulation of energy expenditure (Puigserver et al., 2001). Within a physiological context, Erk, p38 MAPK, and JNK act simultaneously and often times in combination to exert a biological response. Thus, the actions of the MAPKs must be tightly integrated in order to maintain normal physiology. The consequences of the combined actions of altered MAPK signaling that likely occurs in diseases, such as metabolic syndrome, are unknown.

There are 11 members of the classical MKP family all of which inactivate the MAPKs by dephosphorylation. The MKPs have overlapping and distinct sub-cellular localization, expression pattern, and substrate specificity toward the MAPK family members (Camps et al., 2000; Keyse, 2000). MKP-1 is the archetypal member of the cdc25 homology domain-containing MKP family of dual-specificity phosphatases (Camps et al., 2000; Keyse, 2000). MKP-1 was identified as a stress-responsive immediate-early gene following oxidative stress (Keyse and Emslie, 1992) and in response to liver regeneration (Mohn et al., 1991). MKP-1 localizes to the nucleus through a LXXLL motif in its amino terminus (Wu et al., 2005), and it contains a carboxyl

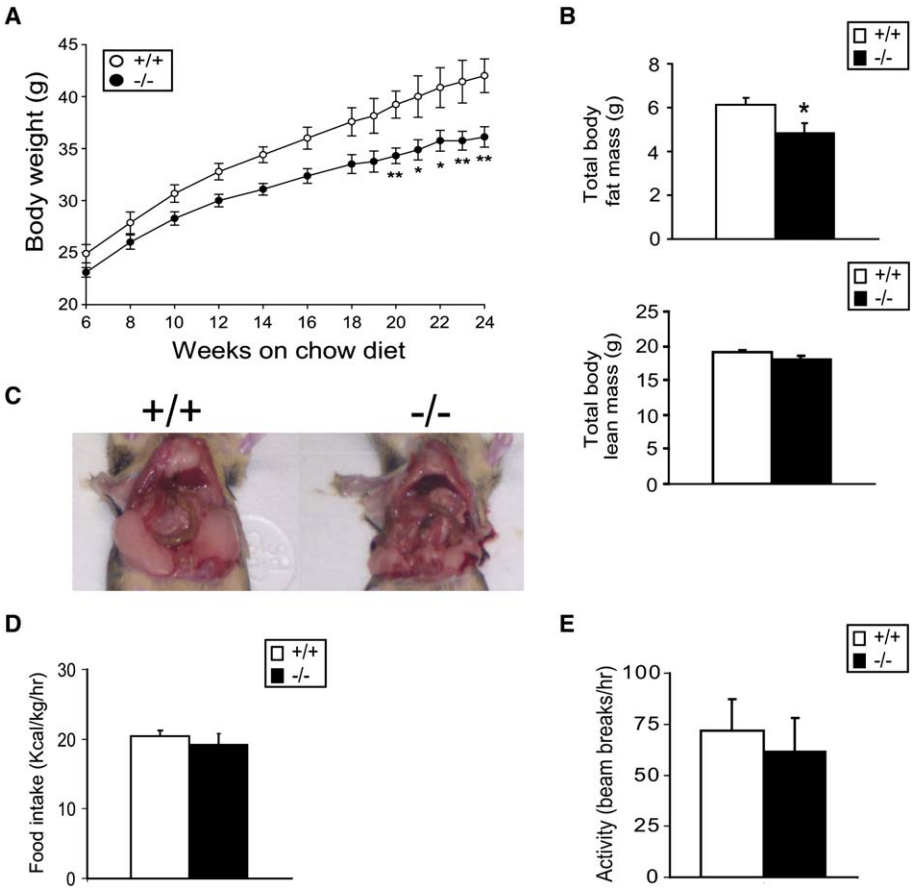

Figure 1. *mkp-1*$^{-/-}$ mice are lean due to reduced body adiposity

A) Analysis of body weight of male *mkp-1*$^{+/+}$ (n = 7–10) and *mkp-1*$^{-/-}$ (n = 9–11) littermates on a chow diet.

B) Whole-body adiposity and lean mass of 13- to 16-week-old male *mkp-1*$^{+/+}$ (n = 17) and *mkp-1*$^{-/-}$ (n = 15) mice.

C) Representative image of abdominal adiposity in 10-month-old *mkp-1*$^{+/+}$ and *mkp-1*$^{-/-}$ littermates.

D) Food consumption in *mkp-1*$^{+/+}$ (n = 6) and *mkp-1*$^{-/-}$ (n = 7) mice.

E) Activity of *mkp-1*$^{+/+}$ (n = 6) and *mkp-1*$^{-/-}$ (n = 7) mice. Data shown are mean ± SEM (*; $p < 0.05$, **; $p < 0.01$).

terminus phosphatase domain. Several groups have shown that cells derived from MKP-1-deficient mice exhibit enhanced p38 MAPK, JNK and Erk activities in response to various stimuli (Nimah et al., 2005; Wu and Bennett, 2005; Zhao et al., 2004). In addition, mice lacking MKP-1 are sensitive to LPS-induced endotoxemia suggesting that MKP-1 plays an important role in the innate immune response (Chi et al., 2006; Hammer et al., 2006; Salojin et al., 2006; Zhao et al., 2006). MKP-1 has been suggested to be involved in obesity and diabetes. In mice, MKP-1 is overexpressed following a HFD (Reddy et al., 2004) as well as in a rat model of diabetes (Chin et al., 1995), whether MKP-1 plays a physiological role in regulating metabolic homeostasis remains to be determined.

Here we show that mice lacking MKP-1 have enhanced MAPK activity in insulin-responsive tissues. MKP-1-deficient mice are lean and exhibit increased levels of energy expenditure in the context of unimpaired insulin action. These data define MKP-1 as a physiological regulator of metabolic homeostasis and additionally reveal some unexpected complexities as to how spatial integration of the MAPK pathways influence metabolism.

Results

mkp-1$^{-/-}$ mice are lean due to reduced body adiposity

Wild-type (*mkp-1*$^{+/+}$), heterozygotic (*mkp-1*$^{+/-}$) and homozygotic (*mkp-1*$^{-/-}$) mice for MKP-1 were born at the expected Mendelian frequency as reported previously (Dorfman et al., 1996). Genotyping of *mkp-1*$^{+/+}$, *mkp-1*$^{+/-}$ and *mkp-1*$^{-/-}$ mice confirmed the presence of the neomycin cassette insertion within exon 2 of either one or both alleles of *mkp-1*$^{+/-}$ and *mkp-1*$^{-/-}$ mice, respectively (Wu and Bennett, 2005). Although no significant differences in pre-weaning weights were observed between *mkp-1*$^{+/+}$ and *mkp-1*$^{-/-}$ mice (Figure S1 in the Supplemental Data available with this article online), when male *mkp-1*$^{-/-}$ mice were weaned on to a chow diet they gained weight at a slower rate than *mkp-1*$^{+/+}$ littermates (Figure 1A), and by 20 weeks of age, *mkp-1*$^{-/-}$ mice gained significantly ($p < 0.01$) less weight than *mkp-1*$^{+/+}$ littermates (Figure 1A). This disparity in body mass became exacerbated as these mice aged, such that by 24 weeks of age, *mkp-1*$^{-/-}$ mice weighed 14% ($p < 0.001$) less than *mkp-1*$^{+/+}$ littermates (Figure 1A). Female *mkp-1*$^{-/-}$ mice were also resistant to weight gain on a chow diet, albeit to a lesser extent than males (Figure S2). To investigate the etiology of the reduced body mass in *mkp-1*$^{-/-}$ mice we performed spectroscopic imaging to measure whole body fat and lean mass. *mkp-1*$^{-/-}$ mice exhibited 21% less fat mass ($p < 0.05$), but lacked significant ($p > 0.1$) differences in lean mass, as compared with *mkp-1*$^{+/+}$ mice (Figure 1B). By 10 months of age, *mkp-1*$^{-/-}$ mice were visibly leaner, and accumulated dramatically reduced amounts of abdominal adiposity (Figure 1C). Despite the observation that *mkp-1*$^{-/-}$ mice were lean they consumed an equivalent amount of food as *mkp-1*$^{+/+}$ controls (Figure 1D), and exhibited comparable levels of locomotor activity (Figure 1E). These results indicate that the reduced adiposity observed in *mkp-1*$^{-/-}$ mice was unlikely to be due either to diminished food consumption or increased

locomotor activity. Thus, mice lacking MKP-1 expression appear to be resistant to weight gain due to reduced body adiposity.

Consistent with the marked reduction in total body adiposity, epididymal fat pads isolated from *mkp-1*$^{-/-}$ mice were significantly smaller by 37% ($p < 0.05$) as compared with *mkp-1*$^{+/+}$ mice (Figure 2A). We performed morphometric analyses on white adipose tissue (WAT) sections to determine the cross-sectional area of adipocytes. Consistent with the decrease in epididymal fat pad mass (Figure 2A), there was a 39% ($p < 0.05$) decrease in the mean cross-sectional area of adipocytes isolated from *mkp-1*$^{-/-}$ mice as compared with *mkp-1*$^{+/+}$ mice (Figures 2B and 2C). These observations imply that *mkp-1*$^{-/-}$ mice have reduced fat pad mass as a consequence of diminished adipocyte lipid content. To link MKP-1 to this altered body composition we measured the activities of the MAPKs in the epididymal fat pads of *mkp-1*$^{+/+}$ and *mkp-1*$^{-/-}$ mice. We found that p38 MAPK, JNK and Erk were all hyper-activated by ~2-fold in WAT from *mkp-1*$^{-/-}$ mice as compared with *mkp-1*$^{+/+}$ mice (Figure 2D, left panel) and that MAPK expression levels were not altered in *mkp-1*$^{-/-}$ mice (Figure 2D, right panel). These results demonstrate that MKP-1 plays a major role in the dephosphorylation of the MAPKs in WAT and suggest that MKP-1 is important for the regulation of adipocyte lipid metabolism.

To investigate the nature of the reduced fat pad mass we asked whether MKP-1 was involved in promoting adipogenesis. Primary mouse embryo fibroblasts (MEFs) derived from *mkp-1*$^{+/+}$ and *mkp-1*$^{-/-}$ mice were induced to undergo adipogenesis. The extent of adipogenesis in *mkp-1*$^{+/+}$ and *mkp-1*$^{-/-}$ MEFs was visualized by staining with Oil red O for the accumulation of lipid. As shown in Figure 2E, both *mkp-1*$^{+/+}$ and *mkp-1*$^{-/-}$ MEFs were equally efficient at undergoing adipogenic conversion as measured by assessing lipid content. Thus, in this setting MKP-1 does not appear to be critical for adipocyte differentiation.

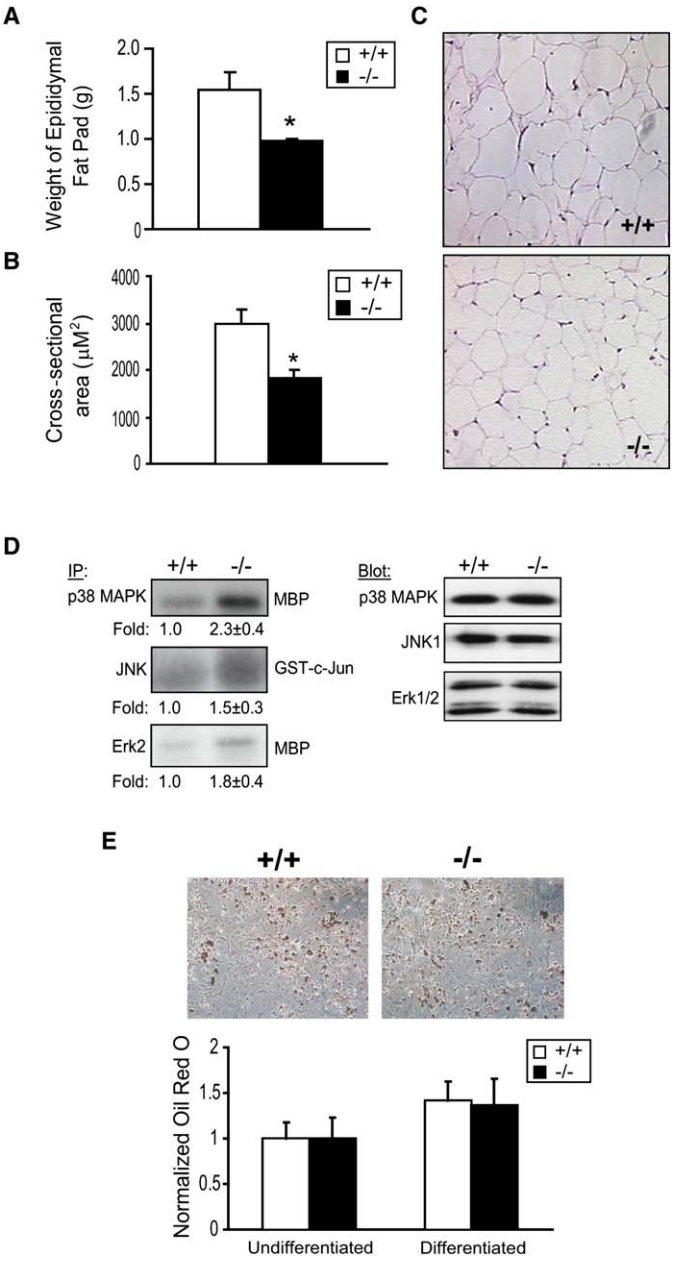

Figure 2. Enhanced white adipose tissue MAPK activity and reduced adipocyte size in *mkp-1*$^{-/-}$ mice

A) Weight of epididymal fat pads from 13- to 16-week-old male *mkp-1*$^{+/+}$ (n = 8) and *mkp-1*$^{-/-}$ (n = 6) mice maintained on a chow diet.

B) Cross-sectional area of adipocytes from *mkp-1*$^{+/+}$ (n = 6) and *mkp-1*$^{-/-}$ (n = 5) mice. Data shown (**A** and **B**) are mean ± SEM (*; $p < 0.05$).

C) Representative histological sections of epididymal fat pads.

D) Left panel: p38 MAPK, JNK and Erk2 activity assays in WAT from *mkp-1*$^{+/+}$ and *mkp-1*$^{-/-}$ mice. The mean ± SEM (n = 4–10) fold-change of MAPK activity as determined by densitometric analyses is shown below each representative autoradiograph. Right panel: total p38 MAPK, JNK1, and Erk1/2 levels in fat pads of *mkp-1*$^{+/+}$ and *mkp-1*$^{-/-}$ mice.

E) Differentiation of primary *mkp-1*$^{+/+}$ and *mkp-1*$^{-/-}$ MEFs showing representative photomicrographs of Oil Red O-stained MEFs and below quantitative assessment of Oil Red O staining from three separate experiments (mean ± SEM).

Regulation of hepatic lipid metabolism and PPARα activity by MKP-1

The livers of young *mkp-1*$^{-/-}$ mice were not markedly different in size to *mkp-1*$^{+/+}$ mice (Figure 3A). However, in aged mice, we found that the livers of *mkp-1*$^{-/-}$ mice did not increase in mass and were up to 25% ($p < 0.001$) smaller than *mkp-1*$^{+/+}$ mice (Figure 3A). In addition, *mkp-1*$^{-/-}$ mice contained 36% less hepatic triglycerides ($p = 0.06$) than *mkp-1*$^{+/+}$ mice (Figure 3B). Livers of aged *mkp-1*$^{-/-}$ mice (~10 months) were markedly reduced in the amount of lipid content as compared with *mkp-1*$^{+/+}$ littermates (Figure 3C), suggesting that *mkp-1*$^{-/-}$ mice are resistant to the acquisition of a fatty liver on a chow diet. The activities of the MAPKs in the livers of *mkp-1*$^{+/+}$ and *mkp-1*$^{-/-}$ mice were measured. p38 MAPK and JNK were found to be hyper-activated by ~2-3 fold in the livers of *mkp-1*$^{-/-}$ mice (Figure 3D, left panel). Erk activity was slightly, but consistently, reduced in *mkp-1*$^{-/-}$ mice as compared with *mkp-1*$^{+/+}$ littermates (Figure 3D, left panel). No differences in the expression of these MAPKs were observed in the livers of *mkp-1*$^{-/-}$ mice (Figure 3D, right panel). The observation that *mkp-1*$^{-/-}$ mice were resistant to the accumulation of hepatic triglycerides, suggested that these mice could have increased levels of hepatic fatty acid oxidation. Consistent with this, upon fasting *mkp-1*$^{-/-}$ mice had increased expression levels (~2-fold) of the liver isoform of carnitine palmitoyltransferase I (Figure 3E), a key rate-limiting enzyme in the hepatic fatty acid β-oxidation pathway. Thus, in the liver, MKP-1 functions as a major MKP for the inactivation

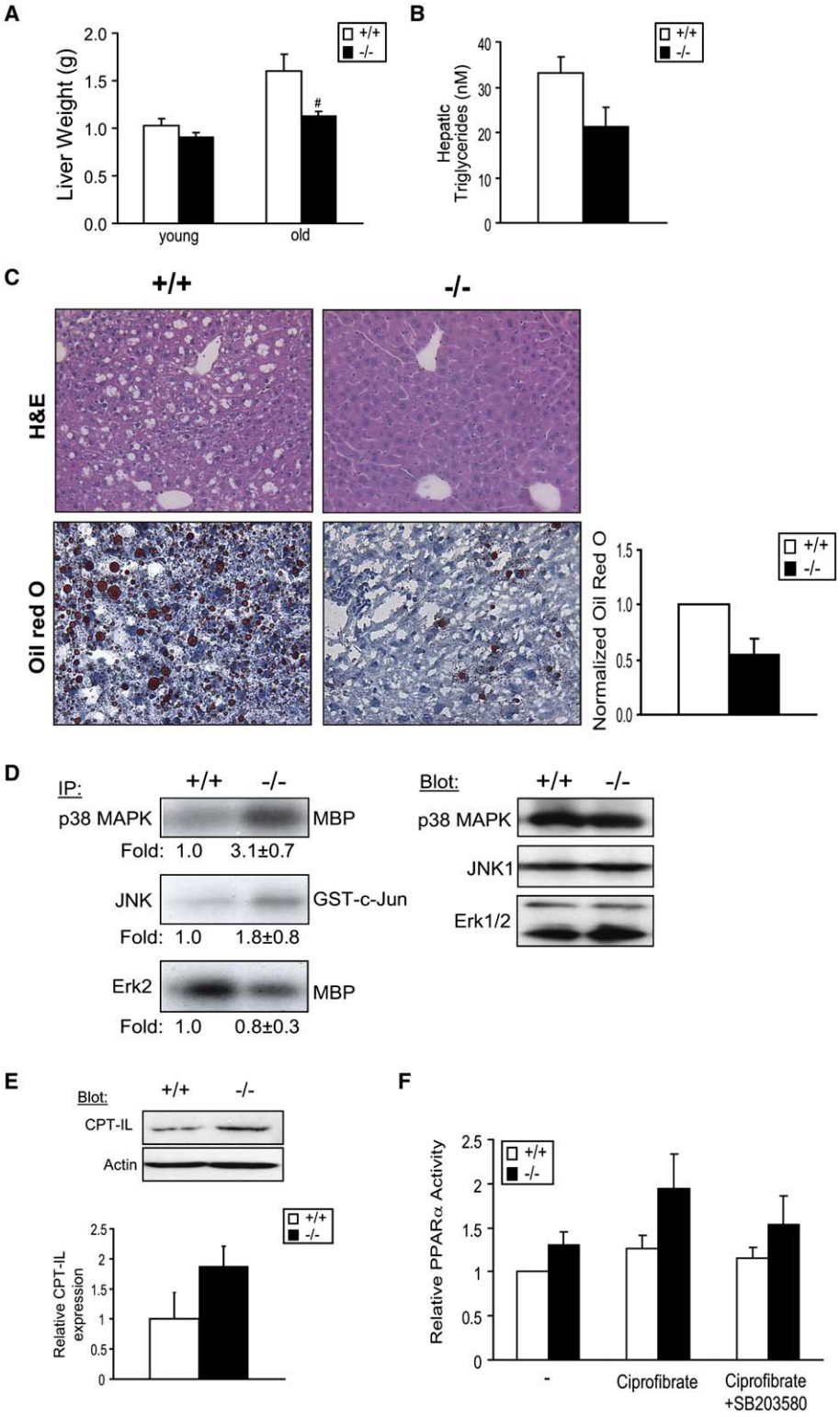

Figure 3. Regulation of hepatic lipid metabolism and PPARα activation by MKP-1

A) Liver weights were determined from 11- to 16-week-old male *mkp-1*$^{+/+}$ (n = 4) and *mkp-1*$^{-/-}$ (n = 5) mice (young) and 28- to 40-week-old male *mkp-1*$^{+/+}$ (n = 9) and *mkp-1*$^{-/-}$ (n = 13) mice (old).

B) Hepatic triglyceride levels were determined from livers isolated from 13- to 17-week-old *mkp-1*$^{+/+}$ (n = 7) and *mkp-1*$^{-/-}$ (n = 5) male mice.

C) Representative histological analysis of liver sections from 6-month-old male *mkp-1*$^{+/+}$ and *mkp-1*$^{-/-}$ littermates (upper panel) and Oil-red-O (lower panel) staining. Graph (*right*) shows quantitation of Oil-red-O staining as a fold difference between male *mkp-1*$^{+/+}$ (n = 4) relative to littermate *mkp-1*$^{-/-}$ mice (n = 4). Data shown (**A**–**C**) are mean ± SEM (#; $p < 0.001$).

D) Left panel: p38 MAPK, JNK and Erk2 activity assays in livers from *mkp-1*$^{+/+}$ and *mkp-1*$^{-/-}$ mice. The mean ± SEM (n = 4–10) fold-change of MAPK activity as determined by densitometric analyses is shown below each representative autoradiograph. Right panel: total p38 MAPK, JNK1 and Erk1/2 levels in livers of *mkp-1*$^{+/+}$ and *mkp-1*$^{-/-}$ mice.

E) Representative immunoblot of CPT-IL expression in the liver of fasted *mkp-1*$^{+/+}$ and *mkp-1*$^{-/-}$ mice. Below is the corresponding densitometric analysis of the relative expression levels of CPT-1L normalized to actin (mean ± SEM) from *mkp-1*$^{+/+}$ (n = 5) and *mkp-1*$^{-/-}$ (n = 6) mice.

F) Primary hepatocytes isolated from *mkp-1*$^{+/+}$ and *mkp-1*$^{-/-}$ mice were transfected with $(ACO)_3$-TK-Luc and *Renilla*. Hepatocytes were either left untreated (–) or were treated with ciprofibrate (200 μM) or ciprofibrate (200 μM) plus SB203580 (5 μM). Data represents the mean fold-change ± SEM from four separate experiments.

of p38 MAPK and JNK and it also regulates hepatic lipid metabolism.

In the liver, the peroxisome proliferator-activated receptor-α (PPARα) (Vega et al., 2000) plays an important role in regulating the expression of genes involved in hepatic triglyceride metabolism. It has been suggested that PPARα activity can be regulated in the nucleus by p38 MAPK which phosphorylates PPARα to increase its sensitivity to ligand-mediated activation and co-activation by the PPARγ co-activator-1 (PGC-1) (Barger et al., 2001). Because MKP-1 appears to negatively regulate p38 MAPK in the liver (Figure 3D), we hypothesized that it could function to attenuate p38 MAPK, and subsequently, PPARα activity and sensitivity to ligand-mediated activation. To test this, a PPARα response element identified in the rat acyl CoA oxidase

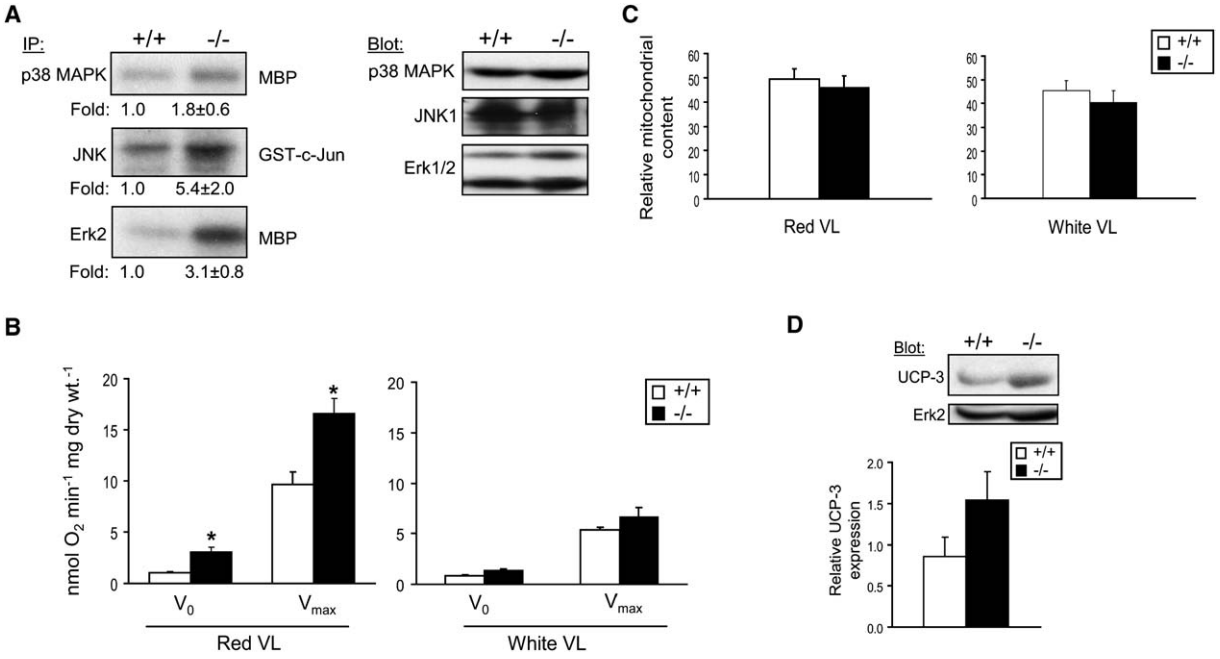

Figure 4. Enhanced MAPK activity and mitochondrial oxygen consumption in skeletal muscle of *mkp-1*$^{-/-}$ mice

A) Left panel: p38 MAPK, JNK and Erk2 activity assays in skeletal muscle from *mkp-1*$^{+/+}$ and *mkp-1*$^{-/-}$ mice. The mean ± SEM (n = 4–10) fold-change of MAPK activity as determined by densitometric analyses is shown below each representative autoradiograph. Right panel: total p38 MAPK, JNK1, and Erk1/2 levels in skeletal muscle of *mkp-1*$^{+/+}$ and *mkp-1*$^{-/-}$ mice.

B) Basal oxygen consumption rate (V_o) and maximal oxygen consumption rates (V_{max}) were measured from high oxidative (red) or low oxidative (white) portions of the vastus lateralis (VL) muscle isolated from 12- to 14-week-old *mkp-1*$^{+/+}$ (n = 3) and *mkp-1*$^{-/-}$ littermates (n = 3).

C) Real-time quantitative PCR represented as arbitrary levels of mitochondrial DNA normalized to skeletal muscle nuclear DNA in red and white VL muscle from *mkp-1*$^{+/+}$ (n = 5) and *mkp-1*$^{-/-}$ mice (n = 5).

D) Tissue homogenates prepared from the gastrocnemius of fasted *mkp-1*$^{+/+}$ and *mkp-1*$^{-/-}$ (11-14 weeks) male mice were subjected to immunoblot analyses with anti-UCP-3 antibody. Results shown are the mean ± SEM of fold-change in UCP-3 expression normalized to Erk2 from *mkp-1*$^{+/+}$ (n = 5) and *mkp-1*$^{-/-}$ (n = 4) mice.

(ACO) promoter fused to luciferase, $(ACO)_3$-TK-luc (Barger et al., 2000; Barger et al., 2001), was transfected into hepatocytes derived from *mkp-1*$^{+/+}$ and *mkp-1*$^{-/-}$ mice. Basal PPARα activity was found to be consistently higher by ~30% in hepatocytes derived from *mkp-1*$^{-/-}$ mice (Figure 3F). We then determined whether PPARα activity in hepatocytes of *mkp-1*$^{-/-}$ mice is sensitized to ligand-mediated activation. The PPARα agonist, ciprofibrate, increased PPARα activity by ~30% in hepatocytes derived from *mkp-1*$^{+/+}$ mice relative to untreated controls (Figure 3F). Whereas, hepatocytes derived from *mkp-1*$^{-/-}$ mice when treated with ciprofibrate exhibited an increase in PPARα activity that was nearly 2-fold higher than ciprofibrate-treated *mkp-1*$^{+/+}$ hepatocytes (Figure 3F). Importantly, treatment of hepatocytes with the p38 MAPK inhibitor, SB203580, attenuated ciprofibrate-induced PPARα activity in hepatocytes derived from *mkp-1*$^{-/-}$ mice. These results suggest that MKP-1 negatively regulates the sensitivity of PPARα to respond to ligand-induced activation by dephosphorylating p38 MAPK.

Enhanced mitochondrial respiration in skeletal muscle of *mkp-1*$^{-/-}$ mice

We next attempted to determine the mechanism through which *mkp-1*$^{-/-}$ mice could be resistant to weight gain. Given that *mkp-1*$^{-/-}$ mice do not appear to have reduced food intake (Figure 1D), we speculated that these mice could be resistant to weight gain due to enhanced energy consumption. We first examined the activities of the MAPKs in skeletal muscle of *mkp-1*$^{+/+}$ and *mkp-1*$^{-/-}$ mice. These results demonstrated that p38 MAPK, JNK and Erk were all hyper-activated in the skeletal muscle of *mkp-1*$^{-/-}$ mice as compared with *mkp-1*$^{+/+}$ mice (Figure 4A, left panel) while no differences in the expression of these MAPKs in skeletal muscle were observed (Figure 4A, right panel). These data demonstrate that MKP-1 is also a major MKP that inactivates the MAPKs in skeletal muscle.

In order to directly assess whether regulation of the MAPKs by MKP-1 was linked to increased mitochondrial efficiency, and thus enhanced energy consumption in *mkp-1*$^{-/-}$ mice, we measured mitochondrial respiration in permeabilized skeletal muscle fibers (Anderson and Neufer, 2006). Muscles from both red and white vastus lateralis were dissected from *mkp-1*$^{+/+}$ and *mkp-1*$^{-/-}$ mice and mitochondrial respiration was measured in the absence (V_0) and presence (V_{max}) of ADP. We found that basal (V_0) and maximal (V_{max}) mitochondrial oxygen consumption were enhanced in red (oxidative) portions of skeletal muscle from *mkp-1*$^{-/-}$ mice as compared with *mkp-1*$^{+/+}$ littermates (Figure 4B). The enhanced levels of mitochondrial oxygen consumption could be due simply to an increase in skeletal muscle mitochondrial content in *mkp-1*$^{-/-}$ mice. However, using real-time quantitative PCR for mitochondrial DNA, as a measure of mitochondrial content, no differences were observed between *mkp-1*$^{+/+}$ and *mkp-1*$^{-/-}$ mice (Figure 4C). Additionally, citrate synthase activity, another marker of mitochondrial content was also similar in skeletal muscles of *mkp-1*$^{+/+}$ and *mkp-1*$^{-/-}$ mice (data not shown). These findings indicate that the increased levels of mitochondrial respiration in skeletal muscles of *mkp-1*$^{-/-}$ mice is unlikely to be associated with elevated

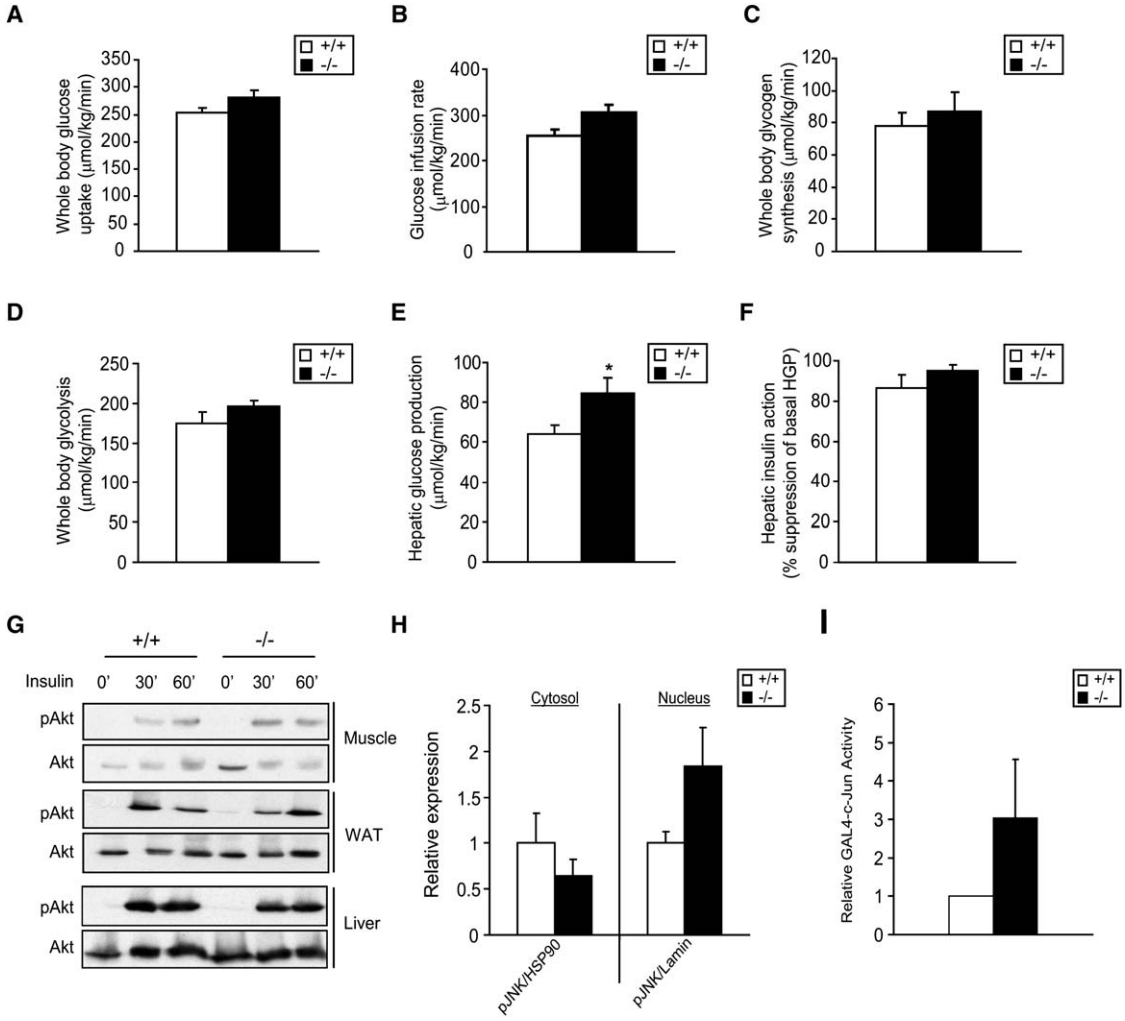

Figure 5. Unaltered insulin-mediated glucose homeostasis and Akt activity in *mkp-1*$^{-/-}$ mice

mkp-1$^{+/+}$ and *mkp-1*$^{-/-}$ mice (13–17 weeks) were subjected to hyperinsulinermic-euglycemic clamp experiments. (**A**) Whole-body glucose uptake, (**B**) glucose infusion rates, (**C**) glycogen synthesis, (**D**) glycolysis, (**E**) hepatic glucose production, and (**F**) % insulin suppression of hepatic glucose production. Data represent mean ± SEM from *mkp-1*$^{+/+}$ (n = 12) and *mkp-1*$^{-/-}$ (n = 11) mice. (**G**) Immunoblot analyses with anti-phospho-Akt and anti-Akt antibodies from skeletal muscle (gastrocnemius), liver and WAT of *mkp-1*$^{+/+}$ and *mkp-1*$^{-/-}$ mice injected i.p. with saline (0') or 0.2 U/kg insulin for 30 or 60 min. (**H**) Nuclear and cytosolic fractions of liver homogenates from 15-week high-fat fed *mkp-1*$^{+/+}$ and *mkp-1*$^{-/-}$ mice were immunoblotted with anti-phospho-JNK, Lamin β1, and HSP90 antibodies. The results shown are the mean ± SEM of the relative change in phospho-JNK levels normalized to HSP90 and Lamin β1 levels for cytosol and nuclear fractions, respectively from *mkp-1*$^{+/+}$ (n = 6) and *mkp-1*$^{-/-}$ (n = 6) mice. (**I**) GAL4-c-Jun and 5xGAL4 luciferase were transfected into *mkp-1*$^{+/+}$ and *mkp-1*$^{-/-}$ hepatocytes along with pRL-*Renilla*. Luciferase normalized to *Renilla* was measured 18 hr later. Data represent the mean ± SEM from 3 separate experiments.

mitochondrial content. To determine further whether MKP-1 alters mitochondrial efficiency, we measured the expression levels of uncoupling protein 3 (UCP-3), a mitochondrial inner membrane protein with a putative role in uncoupling electron transport from oxidative phosphorylation (Esteves and Brand, 2005). Consistent with the elevated respiration in skeletal muscle, levels of UCP-3 protein were increased ~1.5-fold in *mkp-1*$^{-/-}$ mice as compared with *mkp-1*$^{+/+}$ mice on a chow diet (Figure 4D). Taken together, these results suggest that MKP-1 negatively regulates mitochondrial respiration in skeletal muscle.

Unimpaired insulin-mediated glucose homeostasis and enhanced activation of nuclear JNK in *mkp-1*$^{-/-}$ mice

We performed hyperinsulinemic-euglycemic clamp experiments to determine whether chow fed *mkp-1*$^{-/-}$ mice had altered insulin sensitivity. As compared with *mkp-1*$^{+/+}$ mice no significant difference in insulin-stimulated whole body glucose turnover or glucose infusion rates in *mkp-1*$^{-/-}$ mice was observed (Figures 5A and 5B). Consistent with this, both whole body non-oxidative glucose metabolism and glycolysis were unaltered in *mkp-1*$^{-/-}$ mice as compared with *mkp-1*$^{+/+}$ mice (Figures 5C and 5D). Basal hepatic glucose production, however, was significantly enhanced in *mkp-1*$^{-/-}$ mice (Figure 5E), but the ability of insulin to suppress hepatic glucose production was comparable between *mkp-1*$^{+/+}$ and *mkp-1*$^{-/-}$ mice (Figure 5F).

JNK negatively regulates insulin-mediated stimulation of Akt by phosphorylating the insulin receptor substrate-1 (IRS-1) resulting in the attenuation of IRS-1 tyrosyl phosphorylation (Aguirre et al., 2000; Lee et al., 2003). Our data show that although *mkp-1*$^{-/-}$ mice had elevated JNK activity they were not significantly altered in their ability to regulate glucose

homeostasis (Figures 5A–5F). Because MKP-1 is localized to the nucleus (Wu et al., 2005), its actions are presumably restricted to the pool of activated MAPKs that translocate there. Thus, we hypothesized that insulin-mediated Akt activation is unlikely to be affected in *mkp-1*$^{-/-}$ mice. Following an intraperitoneal injection of insulin, skeletal muscle, WAT, and liver were removed from *mkp-1*$^{+/+}$ and *mkp-1*$^{-/-}$ mice and examined for Akt activation. Insulin-mediated Akt activation was not perturbed in skeletal muscle, WAT, or liver from *mkp-1*$^{-/-}$ mice (Figure 5G). These results were consistent with the observation that in the liver, insulin-mediated IRS-1 tyrosyl phosphorylation was comparable between *mkp-1*$^{+/+}$ and *mkp-1*$^{-/-}$ mice (Figure S3). Next, we performed cellular fractionation experiments to determine which pool of JNK was hyper-activated in *mkp-1*$^{-/-}$ mice. To enhance JNK activity we used mice that were fed a HFD for 15 weeks (Hirosumi et al., 2002). Following cytosolic and nuclear fractionation, we found that there was an increase in the amount of phosphorylated JNK in the nucleus, with a concomitant but slight decrease of phosphorylated JNK in the cytosol, from livers of *mkp-1*$^{-/-}$ mice as compared with *mkp-1*$^{+/+}$ mice (Figure 5H). As a surrogate read-out for JNK activity in the nucleus, a c-Jun-GAL4 chimera was transfected into *mkp-1*$^{+/+}$ and *mkp-1*$^{-/-}$ hepatocytes along with GAL4-luciferase to measure JNK-mediated phosphorylation and activation of the transcription factor, c-Jun. Consistent with the fractionation experiments, JNK-mediated activation of c-Jun was increased by ~3 fold in *mkp-1*$^{-/-}$ hepatocytes (Figure 5I). These data demonstrate that *mkp-1*$^{-/-}$ mice exhibit enhanced JNK activity in the nucleus, but not the cytosol. Hence, MKP-1 dephosphorylates the nuclear pool of JNK, suggesting that the action of MKP-1 on JNK in the nucleus is spatially distinct from the regulation of JNK activity in the cytosol.

mkp-1$^{-/-}$ mice are resistant to diet-induced obesity but not glucose intolerance

Our data demonstrates that *mkp-1*$^{-/-}$ mice are resistant to weight gain on a chow diet (Figure 1) but show no marked differences in insulin sensitivity (Figure 5). Therefore, we tested whether *mkp-1*$^{-/-}$ mice were resistant to diet-induced obesity and the development of glucose intolerance which ensues upon feeding a HFD. When fed a HFD (~55% fat content), we observed that *mkp-1*$^{-/-}$ mice were significantly ($p < 0.001$) resistant to weight gain, primarily due to reduced total body adiposity (Figure S4A) following 12 weeks of feeding (Figures 6A and 6B). *mkp-1*$^{-/-}$ mice also continued to be resistant to the acquisition of a fatty liver on a HFD (Figures S4B and S4C). Female *mkp-1*$^{-/-}$ mice were also significantly resistant to weight gain on a HFD (Figure S4D). Fasting glucose levels on either a chow diet or following 4 weeks on a HFD were not significantly different between *mkp-1*$^{+/+}$ and *mkp-1*$^{-/-}$ mice (Figure 6C). Fasting insulin levels were also similar in *mkp-1*$^{-/-}$ mice as compared with *mkp-1*$^{+/+}$ mice after a 4 week HFD (Figure 6D), suggesting that *mkp-1*$^{-/-}$ mice are equally susceptible to the development of hyperinsulinemia on a HFD. Analyses of serum chemistries for mice on a chow diet revealed that *mkp-1*$^{-/-}$ mice had significantly ($p < 0.05$) reduced free fatty acid and serum triglyceride levels (Table S1). No significant differences were observed between *mkp-1*$^{+/+}$ and *mkp-1*$^{-/-}$ mice when cholesterol, high density lipoprotein and β-hydroxybutyrate were measured (Table S1). However, cholesterol levels of *mkp-1*$^{-/-}$ mice were significantly ($p < 0.05$) lower as compared with *mkp-1*$^{+/+}$ mice following a HFD (Table S1). No significant differences in either leptin or adiponectin levels were observed between *mkp-1*$^{+/+}$ and *mkp-1*$^{-/-}$ mice under chow or after 12 weeks of HFD feeding (Table S1). These results demonstrate that *mkp-1*$^{-/-}$ mice are resistant to diet-induced obesity.

Mkp-1$^{-/-}$ mice showed unimpaired effects of insulin on glucose homeostasis on a chow diet potentially due to the restriction of the activated pool of JNK to the nucleus (Figure 5). Therefore, we hypothesized that *mkp-1*$^{-/-}$ mice when placed on a HFD should be lean and protected from developing glucose intolerance. To test this, we compared glucose tolerance tests (GTT) from *mkp-1*$^{+/+}$ and *mkp-1*$^{-/-}$ mice on a chow diet with those following 4 weeks on a HFD. *mkp-1*$^{-/-}$ mice on a chow diet cleared glucose from the periphery at a slightly lower level of efficiency as compared with *mkp-1*$^{+/+}$ mice although this difference was not statistically significant (Figure 6E). Following 4 weeks on a HFD, both *mkp-1*$^{+/+}$and *mkp-1*$^{-/-}$ mice became significantly ($p < 0.0001$) glucose intolerant (Figure 6E). We found that even after 12 weeks on a HFD when *mkp-1*$^{-/-}$ mice were significantly leaner ($p < 0.001$) as compared with *mkp-1*$^{+/+}$ mice (Figures 6A and 6B), GTT analyses showed that *mkp-1*$^{+/+}$ and *mkp-1*$^{-/-}$ mice became dramatically glucose intolerant to comparable levels (Figure 6E). Collectively, these data provide strong evidence for the uncoupling of diet-induced obesity and glucose intolerance in mice lacking MKP-1 expression.

Enhanced energy expenditure and respiration rate in high fat fed *mkp-1*$^{-/-}$ mice

To further investigate the cause of the resistance to diet-induced obesity in *mkp-1*$^{-/-}$ mice we determined the respiratory rate (VO_2), energy expenditure, respiratory quotient (RQ), and locomotor activity after 15 weeks on a HFD. Energy expenditure and respiratory rate (normalized to body weight) were both significantly higher in *mkp-1*$^{-/-}$ mice as compared with *mkp-1*$^{+/+}$ mice ($p < 0.05$) (Figures 7A and 7B). The utilization of carbohydrate to fat in *mkp-1*$^{-/-}$ mice was equivalent to that of *mkp-1*$^{+/+}$ mice as indicated by their identical RQ levels (Figure 7C). Obese *mkp-1*$^{+/+}$ mice on a HFD were less active than when on a chow diet (Figure 7D and 1E). In contrast, *mkp-1*$^{-/-}$ mice maintained their level of locomotor activity on a HFD as compared to when fed a chow diet (Figure 7D and 1E). These data indicate that *mkp-1*$^{-/-}$ mice are not hyperactive per se, nevertheless their maintained level of locomotor activity on a HFD relative to *mkp-1*$^{+/+}$ mice could contribute to their resistance to diet-induced obesity. Reduced levels of total body adiposity in *mkp-1*$^{-/-}$ mice (Figure S4A) could additionally occur as a result of decreased levels of food consumption. However, when food intake was measured in these HFD fed mice, *mkp-1*$^{-/-}$ mice actually consumed more food as compared to *mkp-1*$^{+/+}$ mice (*mkp-1*$^{+/+}$; 7.2 ± 1.5 Kcal/Kg/h [n = 7] versus *mkp-1*$^{-/-}$; 11.6 ± 3.8 Kcal/Kg/h [n = 6]). Therefore, even though *mkp-1*$^{-/-}$ mice consume more food than *mkp-1*$^{+/+}$ mice on a HFD diet, they remain leaner. These results support the interpretation that *mkp-1*$^{-/-}$ mice are resistant to diet-induced obesity due, in part, to increased levels of energy expenditure.

Discussion

In this report, we show that *mkp-1*$^{-/-}$ mice exhibit enhanced p38 MAPK, JNK and Erk activities in insulin-responsive tissues.

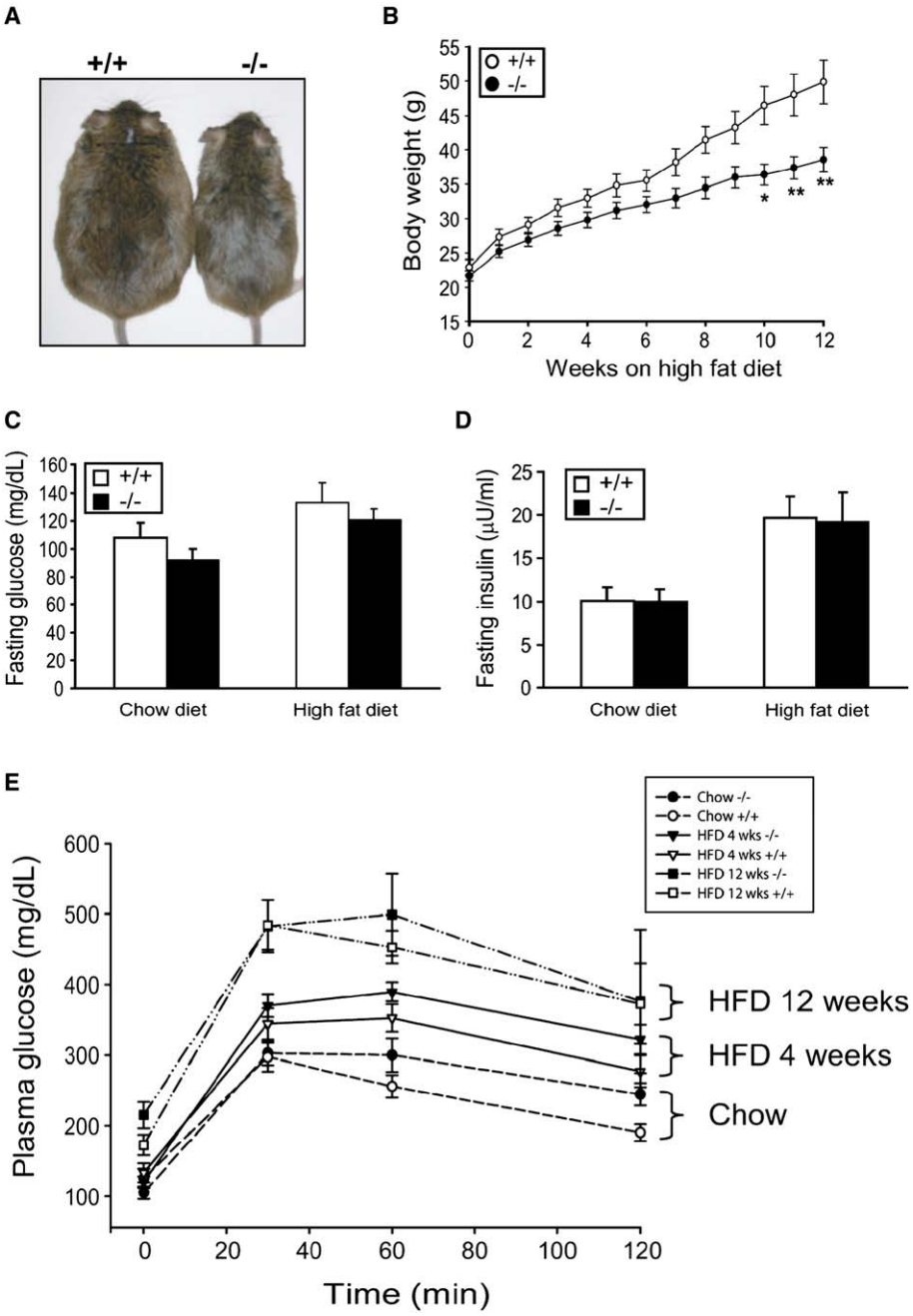

Figure 6. Resistance to HFD-induced obesity but not glucose intolerance in *mkp-1*$^{-/-}$ mice

mkp-1$^{+/+}$ and *mkp-1*$^{-/-}$ mice (5–6 weeks old) were placed on a HFD for 4–12 weeks.

A) Representative image of male *mkp-1*$^{+/+}$ and *mkp-1*$^{-/-}$ mice following a 12-week HFD.

B) Body weight of male *mkp-1*$^{+/+}$ (n = 7) and *mkp-1*$^{-/-}$ (n = 11) mice monitored weekly for 12 weeks (*; $p < 0.05$ and **; $p < 0.01$).

C) Fasting glucose levels from *mkp-1*$^{+/+}$ and *mkp-1*$^{-/-}$ mice on a chow diet or a 4 week HFD (n = 9–14).

D) Fasting insulin levels were determined from *mkp-1*$^{+/+}$ and *mkp-1*$^{-/-}$ mice on a chow diet or a 4 week HFD (n = 12–13).

E) Fasted 10–14 week old mice maintained on a chow diet (*mkp-1*$^{+/+}$ [n = 7–8] and *mkp-1*$^{-/-}$ [n = 8]) or fasted mice that have been on a HFD for 4 weeks (*mkp-1*$^{+/+}$ [n = 9] and *mkp-1*$^{-/-}$ [n = 9]) or 12 weeks (*mkp-1*$^{+/+}$ [n = 5] and *mkp-1*$^{-/-}$ [n = 4]) were subjected to GTTs. Data represent the mean ± SEM. By One-way ANOVA $p < 0.001$; *mkp-1*$^{+/+}$ chow versus *mkp-1*$^{+/+}$ HFD 4 and 12 weeks; *mkp-1*$^{-/-}$ chow versus *mkp-1*$^{-/-}$ HFD 4 and 12 weeks. $p > 0.1$; *mkp-1*$^{+/+}$ versus *mkp-1*$^{-/-}$ on chow, HFD 4 and 12 weeks.

Consistent with their lean phenotype, *mkp-1*$^{-/-}$ mice were protected from diet-induced obesity. Remarkably, although lean and resistant to diet-induced obesity, *mkp-1*$^{-/-}$ mice were not insulin sensitive and were susceptible to the development of glucose intolerance and hyperinsulinemia when fed a HFD. These observations were surprising in context of the role for JNK in promoting obesity and insulin resistance. We resolved this dichotomy by demonstrating that in the absence of MKP-1, JNK activation is enhanced in the nucleus, and not cytosol. Hence, the dephosphorylation of the MAPKs by MKP-1 in the nucleus is spatially and functionally distinct from the regulation of the MAPKs in the cytosol (Figure 7E).

In WAT, liver and skeletal muscle of *mkp-1*$^{-/-}$ mice we found that p38 MAPK and JNK were hyper-activated. Erk was hyper-activated in WAT and skeletal muscle, but not in the liver of *mkp-1*$^{-/-}$ mice. These results demonstrate that MKP-1 is a major physiological regulator of p38 MAPK, JNK and Erk activity in insulin-responsive tissues and that hyper-activation of one or more of these MAPKs are causal to the metabolic phenotype observed in *mkp-1*$^{-/-}$ mice. These *mkp-1*$^{-/-}$ mice have been studied previously but no metabolic defects were reported. One possibility for this is that there could have been differences in the composition of the chow diet used in the previous study (Dorfman et al., 1996). Genetic background is not likely to be a factor given that the mice used in this study were derived from the original strain (Dorfman et al., 1996). However, we cannot rule-out the possibility that the mixed genetic background to which these mice were bred could be a contributing factor to the phenotype.

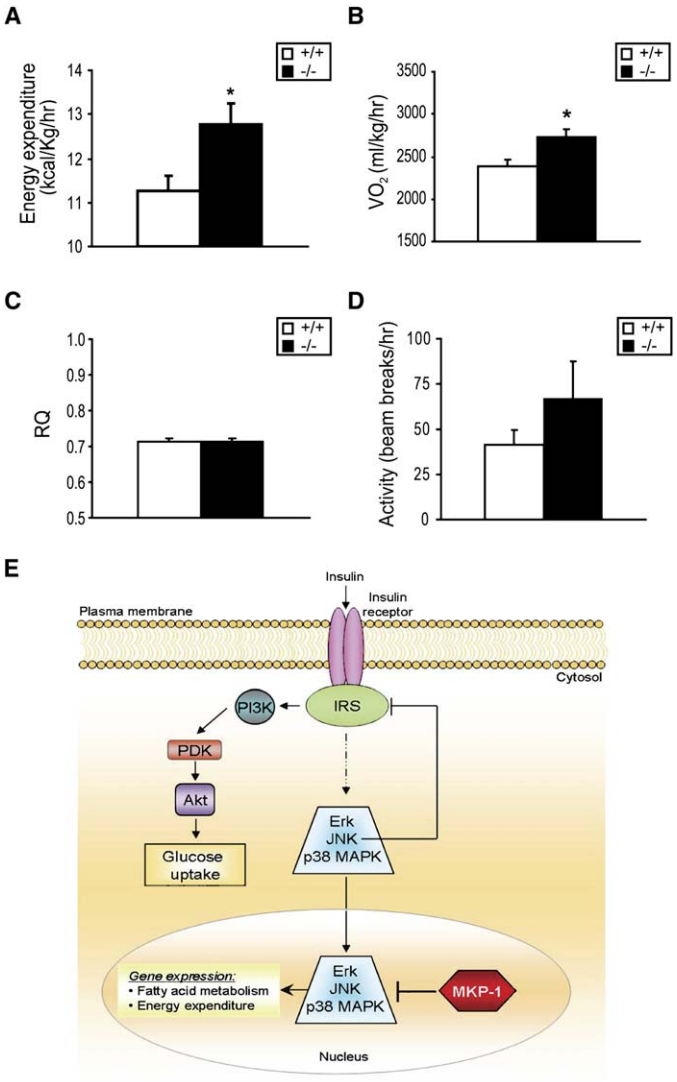

Figure 7. Enhanced energy expenditure and oxygen consumption in *mkp-1*$^{-/-}$ mice

mkp-1$^{+/+}$ and *mkp-1*$^{-/-}$ mice fed a HFD for 15 weeks were subjected to open circuit calorimetry. (**A**) Energy expenditure, (**B**) oxygen consumption, (**C**) respiratory quotient (RQ), and (**D**) activity were measured. Graphs represent the mean ± SEM for *mkp-1*$^{+/+}$ (n = 7) and *mkp-1*$^{-/-}$ (n = 6) mice (*;p < 0.05). (**E**) Model depicting the nuclear inactivation of the MAPKs by MKP-1 in the control of gene expression events involved in fatty acid metabolism and energy expenditure. In the cytosol the MAPKs are regulated independently of MKP-1.

The importance of the MAPKs in metabolic homeostasis has been demonstrated previously. Hyper-activation of JNK is implicated in insulin resistance (Hirosumi et al., 2002), whereas p38 MAPK has been shown to be involved in the positive regulation of energy expenditure (Puigserver et al., 2001). Erk-1-deficient mice were shown to be resistant to diet-induced obesity and were protected from the development of insulin resistance (Bost et al., 2005). It is clear that each of these individual MAPKs can affect metabolic regulation. However, in the absence of MKP-1, both p38 MAPK and JNK, and in some cases, Erk are all hyper-activated in the same tissue. Thus, the phenotype observed in *mkp-1*$^{-/-}$ mice is not a simple recapitulation of hyper-activation of each of these individual MAPKs but rather, represents a unique phenotype depicting the combined actions of hyper-activation of either one, two or all three of the MAPKs. The complexity of the interplay amongst the MAPKs is further highlighted by evidence indicating that the MAPKs exhibit cross-talk. For example, it has been shown that both p38 MAPK and JNK can negatively regulate Erk activity (Shen et al., 2003; Zhang et al., 2001). In this regard, cross-talk between the MAPKs might explain the paradoxical decrease in Erk activity in the liver when both p38 MAPK and JNK were hyper-activated in *mkp-1*$^{-/-}$ mice. The results presented here emphasize the physiological specificity within the family of MKPs. Most noteworthy, are the differences, and some similarities, between our results and mice deficient in other MKPs. For example, MKP-4 knock-out mice are embryonic lethal (Christie et al., 2005). In contrast, we and others have shown recently that MKP-1 is involved in the regulation of innate immunity (Chi et al., 2006; Hammer et al., 2006; Salojin et al., 2006; Zhao et al., 2006) similar to that of MKP-5 (Zhang et al., 2004). Taken together with our results these studies clearly establish that the MKPs engage in non-redundant physiological functions.

We found that mice lacking MKP-1 have reduced adiposity attributed, at least in part, to smaller adipocyte size. This suggests that MKP-1 regulates pathways that control lipid homeostasis. It is conceivable that hyper-activation of Erk and/or JNK in adipocytes of mice lacking MKP-1 impairs PPARγ-mediated lipogenesis. Alternatively, *mkp-1*$^{-/-}$ mice might have reduced fat mass because of fewer adipocytes. MKP-1 has been implicated in the positive regulation of adipogenesis in pre-adipocytes (Sakaue et al., 2004). Contrary to those data, however, we found unaltered adipogenesis in primary MEFs isolated from *mkp-1*$^{-/-}$ mice. What is interesting is the observation that despite the significant disparity in fat mass, *mkp-1*$^{-/-}$ mice displayed equivalent levels of leptin to *mkp-1*$^{+/+}$ mice. We speculate that enhanced MAPK activity in *mkp-1*$^{-/-}$ mice might increase leptin expression in context of a lean phenotype to levels comparable to that observed in *mkp-1*$^{+/+}$ mice. Indeed, leptin expression has been shown to be dependent upon Erk activity in certain cell types (Bradley et al., 2002). In addition, we have shown that *mkp-1*$^{-/-}$ mice have elevated levels of a number of cytokines, in particular TNFα (Chi et al., 2006), which can induce the expression of leptin in fat (Sarraf et al., 1997). Transgenic mice overexpressing UCP-3 in skeletal muscle also exhibit dramatically reduced levels of adipose tissue but their levels of leptin are equivalent to that of wild-type mice (Clapham et al., 2000). In line with this, we too observe increased levels of UCP-3 expression in skeletal muscle of *mkp-1*$^{-/-}$ mice.

MKP-1 may indirectly link the regulation of body adiposity through its effect on skeletal muscle metabolism since we demonstrate that it negatively regulates mitochondrial respiration in skeletal muscle. PGC-1α which stimulates the transcription of a number of mitochondrial genes involved in energy expenditure, is a direct target for activation by p38 MAPK (Puigserver et al., 2001). Therefore, the enhanced levels of p38 MAPK activity observed in skeletal muscle may cause increased PGC-1α-mediated expression of genes involved in energy consumption, thereby providing at least one of the contributing factors that promotes the lean phenotype of *mkp-1*$^{-/-}$ mice. At this juncture we cannot exclude contributions from other sites of MKP-1 action that may also regulate energy expenditure. In particular, MKP-1 is expressed in the hypothalamus (Mastaitis et al., 2005), and it may influence MAPK-dependent signaling events

mediated by either insulin and/or leptin at this site. Although it has been suggested that insulin-mediated activation of Erk in the hypothalamus controls sympathetic outflow to skeletal muscle (Rahmouni et al., 2004) which indirectly stimulates energy expenditure, it is not firmly established whether the metabolic effects of leptin in the hypothalamus are dependent upon the activity of the MAPKs. On the contrary, evidence seems to imply that hyper-activation of Erk alone promotes obesity (Bost et al., 2005; Rodriguez et al., 2006). In context of our findings, such results serve to further highlight the complexity of the combinatorial effects of JNK, p38 MAPK and Erk in the control of metabolic homeostasis.

Our results have uncovered an important regulatory role for MKP-1 in hepatic lipid metabolism. Mice lacking MKP-1 were resistant to the acquisition of a fatty liver suggesting that MKP-1 negatively regulates hepatic fatty acid oxidation. Indeed, we observed increased expression levels of the liver isoform of carnitine palmitoyltransferase I in fasted mice lacking MKP-1 expression. Hepatic fatty acid oxidation also proceeds through activation of the PPAR pathway. In this regard, MKP-1 was found to control the sensitivity of PPARα to be activated by ciprofibrate, a PPARα-specific ligand, in a p38 MAPK-dependent manner. It appears reasonable to propose that in the liver, regulation of p38 MAPK by MKP-1 may set the sensitivity of PPARα to become activated by its physiological ligands. In the liver, p38 MAPK has also been implicated in the positive regulation of gluconeogenesis (Cao et al., 2005). We observed that basal hepatic glucose production is increased in *mkp-1*$^{-/-}$ mice correlating with the elevated levels of p38 MAPK. Hepatic insulin action appears intact in the liver under the dose of insulin employed in these clamp studies, as well as in response to the acute actions of insulin on IRS-1 tyrosyl phosphorylation, and Akt activation which were unaffected in the livers of *mkp-1*$^{-/-}$ mice. Hence, we favor the interpretation that the enhanced levels of basal hepatic glucose production is likely due to increased levels of gluconeogenesis rather than being reflective of hepatic insulin resistance.

Typically, leanness correlates with increased insulin sensitivity. Therefore, the most provocative finding of this study is the observation that mice lacking MKP-1 are neither insulin sensitive, even though they are lean, nor protected from the loss of glucose homeostasis as a result of high-fat feeding, but yet are resistant to diet-induced obesity. A similar uncoupling of glucose intolerance following a HFD in context of a lean phenotype has been observed in transgenic mice overexpressing PPARα in skeletal muscle (MCK-PPARα) (Finck et al., 2005). MCK-PPARα mice were suggested to develop glucose intolerance as a consequence of enhanced fatty acid oxidation and importantly, this occurred without any apparent alteration to insulin signaling (Finck et al., 2005). It is possible that the enhanced level of p38 MAPK activity in skeletal muscles of *mkp-1*$^{-/-}$ mice might increase PPARα-mediated fatty acid oxidation, similar to that in the liver, to precipitate an analogous pathophysiological pathway for the development of glucose intolerance following a HFD independently of the effects on insulin signaling.

Despite JNK being elevated in all insulin-responsive tissues in chow fed *mkp-1*$^{-/-}$ mice we found that insulin-mediated glucose regulation as measured by hyperinsulinemic-euglycemic clamp experiments revealed equivalent levels of whole body glucose turnover in *mkp-1*$^{-/-}$ mice as compared to controls. We reasoned that the lack of effect of MKP-1 on whole body insulin-mediated glucose uptake could be due to the fact that MKP-1 is localized to the nucleus (Wu et al., 2005), and thus only regulates that pool of active MAPKs, which either may not interfere with or have access to, cytosolic components of the insulin signaling pathway that control glucose uptake (Figure 7E). Three lines of evidence support this notion. First, neither IRS-1 tyrosyl phosphorylation, which is attenuated by JNK, nor Akt activation in response to insulin, was appreciably altered in *mkp-1*$^{-/-}$ mice. Second, we found that the pool of hyper-activated JNK accumulated in the nucleus of livers derived from *mkp-1*$^{-/-}$ mice. Third, JNK-mediated c-Jun activation was enhanced in the nucleus of *mkp-1*$^{-/-}$ hepatocytes. Together, these results imply that MKP-1 specifically dephosphorylates the nuclear pool of MAPKs, as anticipated, but here we provide direct evidence for this spatially restricted sub-cellular regulation. The consequences of MKP-1 deficiency results in the functional uncoupling of the targets of JNK in the cytosol from those that reside in the nucleus. Although it has been inferred that the discrete sub-cellular localization of the MKPs is important for their physiological function (Volmat et al., 2001), the data described herein provides genetic evidence that this is indeed the case. Increased activity of JNK, and potentially p38 MAPK and Erk in the nucleus might enhance transcriptional activation of genes that are involved in the regulation of fatty acid metabolism and energy expenditure (Figure 7E).

In summary, we demonstrate that MKP-1 plays a major physiological role as a dual-specificity phosphatase for the inactivation of the MAPKs in insulin-responsive tissues. Further, we provide insight into the consequences of the combinatorial actions of enhanced MAPK activity in the progression of metabolic syndrome. By defining MKP-1 as a molecular target that uncouples diet-induced obesity from glucose intolerance raises the possibility that pharmacological inactivation of MKP-1 can be used as a therapy for the specific treatment of obesity.

Experimental procedures

Maintenance of mice

Mice containing a disruption within exon 2 of MKP-1 (*mkp-1*$^{-/-}$) were derived by implantation of heterozygotic (*mkp-1*$^{+/-}$) 129J/C57BL6 embryos obtained from Bristol-Myers Squibb (Princeton, NJ) (Dorfman et al., 1996) into surrogate mothers. All experiments were performed with mice generated from inter-crossed heterozygous breeders. *mkp-1*$^{+/+}$ and *mkp-1*$^{-/-}$ mice were maintained on a rodent chow #2018 (Harlan Teklad, IN). For HFD studies, 5-6 week old male and female mice were placed on TD 93075 (Harlan Teklad) diet for 12-15 weeks. For genotyping, PCR analysis was employed using triple primers consisting of forward primers 5′-CCAGGTACTGTGTCGGT GGTGC-3′ and 5′-CAGCGCATCGCCTTCTATCGCC-3′, with reverse primer 5′-GCTTTCTATATCCTCCTGG-3′.

Isolation of primary cell cultures and adipogenesis assays

Primary mouse embryonic fibroblasts (MEF) were derived as described previously (Wu and Bennett, 2005). For adipogenesis assays, primary MEFs (passage 3-4) were cultured in growth media (Dulbecco's modified Eagle's medium (DMEM; Invitrogen) supplemented with 10% fetal bovine serum (FBS; Sigma, St. Louis, MO), 10 U/ml penicillin (Sigma) and 50 μg/ml streptomycin (Sigma). Two days post confluence, cells were switched to adipogenesis media (DMEM supplemented with 10% FBS, 10 U/ml penicillin, 50 μg/ml streptomycin, 10 μg/ml insulin [Sigma], 5 μM dexamethasone [Sigma], and 0.5 mM 3-Isobutyl-1-methylxanthine [IBMX; Sigma]). Adipogenesis media was changed every 48 hr for 14 days. Cells were washed with phosphate-buffer saline (PBS), fixed in 10% formalin at room temperature for 15 min, and stained with 0.5% Oil-red-O in isopropyl alcohol:distilled water [60:40]

for 30 min at 37ºC. The absorbance of the extracted stain was measured at 510 nm. Primary hepatocytes were isolated using a modified collagenase digestion method as described previously (Boyer et al., 1990). Hepatocytes were cultured in DMEM supplemented with 10% FBS, 50 nM insulin, 1 μM dexamethasone, 1 mM sodium pyruvate, 10 U/ml penicillin and 50 μg/ml streptomycin.

Histological analysis of tissue

WAT was isolated from *mkp-1*$^{+/+}$ and *mkp-1*$^{-/-}$ mice and fixed in 4% paraformaldehyde in PBS and processed for paraffin sections and stained by hematoxylin and eosin. Cross-sectional areas of adipocytes were measured using Image J software by counting at least 300 individual cells from random fields in histological sections. Non-perfused livers were digested in chloroform-methanol to determine hepatic triglyceride levels. Lipid layers were separated using H_2SO_4 and the triglyceride concentration was determined with a triglyceride assay kit (Sigma Diagnostics) according to the manufacturer's instructions. Livers were fixed either in 4% paraformaldehyde-PBS and stained by hematoxylin and eosin, or snapped-frozen in 5-methylbutane (Sigma). Cryostat sections of livers were fixed with 4% paraformaldehyde-PBS for 1 hr and cryoprotected with 20% sucrose prior to staining with 4% Oil Red O for 2 hr. Liver tissues were fixed with 10% formalin in PBS for 2 hr then stained with 4% Oil Red O solution for 2 hr.

Biochemical analysis of tissue

For immune complex kinase assays, liver and gastrocnemius muscle were homogenized with 10 or 20 volumes of homogenizing buffer (25 mM Tris. HCl pH 7.4, 150 mM NaCl, 5 mM EDTA, 1% Triton X-100, 0.1% SDS, 10% glycerol, 1 mM DTT, 0.5 % sodium deoxycholic acid) supplemented with protease and phosphatase inhibitors (5 μg/ml leupeptin, 5 μg/ml aprotinin, 1 μg/ml pepstatin A, 1 mM PMSF, 1 mM benzamidine, 1 mM Na_3VO_3, and 10 mM NaF). WAT was lysed in RIPA buffer (25 mM Tris. HCl pH 7.4, 150 mM NaCl, 5 mM EDTA, 1% NP-40, 0.1 % SDS, 1.0 % sodium deoxycholic acid). Homogenates were lysed for 30 min prior to clarification at 20,800 *g* for 30 min at 4ºC. Protein concentrations were determined by Coomassie Protein Reagent (Pierce, Rockford, IL). Erk2, JNK, or p38 MAPK were immunoprecipitated with anti-Erk2 (Santa Cruz Biotechnology, Santa Cruz, CA), anti-JNK1 (Santa Cruz Biotechnology) or anti-p38 MAPK (Santa Cruz Biotechnology) antibodies, respectively for 4 hr or overnight at 4ºC. Erk2 and JNK1 immune complexes were collected on Protein A Sepharose and Protein G Sepharose was used to capture p38 MAPK immune complexes. Purified GST-c-Jun (amino acids 5-89 of c-Jun) protein was used to precipitate JNK. The complexes were washed with lysis buffer and kinase buffer. The kinase reactions were performed with 50 μl of kinase buffer for 30 min at 30ºC, using 1 μg of myelin basic protein (Sigma) as a substrate for Erk2 or p38 MAPK or 1 μg GST-c-Jun as a substrate for JNK. Reactions were terminated by the addition of sample buffer and substrates were resolved by SDS-PAGE and visualized by autoradiography. Tissue homogenates were resolved by SDS-PAGE and proteins were transferred to Immobilon-P membranes and immunoblotted with antibodies to Erk1/2, JNK, p38 MAPK, the liver isoform of carnitine palmitoyltransferase I (CPT-1L) (Alpha Diagnostic International) or UCP-3 (Calbiochem-Novabiochem). To assess insulin-mediated Akt activation in vivo, 10-14 week old males were fasted overnight and injected intraperitonealy with saline or 0.2 U/kg insulin (Novo Nordisk, Novolin) for 30 or 60 min. WAT, gastrocnemius, and liver were isolated and snap-frozen in liquid nitrogen. Tissue homogenates were prepared and protein was separated on SDS-PAGE and immunoblotted with anti-phospho-Akt and anti-Akt antibodies (Cell Signaling Technology). To assess insulin-mediated IRS-1 tyrosyl phosphorylation, IRS-1 was immunoprecipiated from liver homogenates with IRS-1 antibodies (Santa Cruz Biotechnology), immune complexes were immunoblotted with either anti-IRS-1 or anti-phosphotyrosine (clone 4G10) antibodies.

Sub-cellular Fractionation

Liver fractionation was performed as previously described (Tata et al., 1974) with the following modifications. Sucrose buffers contained 5 μg/ml leupeptin, 5 μg/ml aprotinin, 1 μg/ml pepstatin A, 1 mM benzamidine, 2 mM Na_3VO_3, and 50 mM NaF. The nuclear pellet was resuspended in RIPA buffer (1.0% NP-40, 50 mM Tris-HCl (pH 7.4), 150 mM NaCl, 5 mM EDTA, 0.1% SDS, 1% sodium deoxycholate), along with protease and phosphatase inhibitors. Liver fractions were immunoblotted with phospho-JNK (Cell Signaling Technology), Lamin β1 (Santa Cruz Biotechnology) or HSP-90 (BioVision Inc) antibodies. The amount of phosphorylated JNK was normalized to either HSP-90 or lamin β1 for cytosolic or nuclear fractions, respectively.

Glucose tolerance test and blood chemistry

Overnight fasted 10-14 week old male mice or male mice that have been on a HFD for 4-5 weeks were intraperitonealy injected with D-glucose (20% solution; 1 g/kg body weight). Tail vein blood was collected at 0, 30, 60 and 120 min following glucose injection and blood glucose level was measured with a Beckman Glucose Analyzer 2 (Beckman, Fullerton, CA). Plasma insulin levels were measured by radioimmunoassay using kits from Linco Research (St. Charles, MO). Plasma was collected from overnight fasted mice and the Yale Mouse Metabolic Phenotyping Center was used to determine the plasma concentration of cholesterol, high density lipoprotein, triglyceride, free fatty acid, and β-hydroxybutyrate. Leptin and adiponectin measurements were performed by Linco Research Inc. (St. Charles, Missouri) from mice that were fed either a chow or HFD for 12 weeks. Samples were obtained from mice that were fasted overnight following 1.5 hr re-feeding.

Body composition, hyperinsulinemic-euglycemic clamps and metabolic calorimetry

Whole body fat and lean mass were measured from unanesthetized male mice using ^{1}H-magnetic resonance spectroscopy (Bruker Mini-spec Analyzer; Echo Medical Systems, Houtson, TX). At least 4 days before clamp experiments, whole body fat and lean mass were measured in awake age-matched mice using ^{1}H-MRS. Following the body composition analysis, mice were anesthetized, and surgery was performed to establish an indwelling catheter in the right internal jugular vein (Park et al., 2005). Following an overnight fast, a 2 hr hyperinsulinemic-euglycemic clamp was conducted in awake mice with a continuous infusion of insulin (15 pmol/kg/min; Humulin, Eli Lilly, Indianapolis, IN) and variable infusion of 20% glucose (Park et al., 2005). Basal and insulin-stimulated whole body glucose turnover was estimated with a continuous infusion of [3-^{3}H]glucose (Perkin Elmer Life and Analytical Sciences, Boston, MA) for 2 hr prior to and throughout the clamps (Park et al., 2005). Metabolic measurements for activity, food, and energy expenditure were performed using the Comprehensive Lab Animal Monitoring System (CLAMS: Columbus Instruments, Columbus, OH, USA). During data analysis, energy expenditure and feeding were normalized to body weight. Respiratory quotient (RQ) and energy expenditure were calculated from the gas exchange data. Activity was measured using infrared beams to count the amount of beam breaks during the specified measurement period. Feeding was measured by recording the difference in the scale measurement of the Center-Feeder from one time point to another.

Skeletal muscle mitochondrial respiration and mitochondrial content assays

Mitochondrial oxygen consumption was determined in permeabilized fiber bundles from red and white portions of the vastus lateralis muscle as previously described (Anderson and Neufer, 2006). Briefly, basal (V_o, no ADP) and maximal (V_{max}, 330 μM ADP) respiration supported by pyruvate (500 μM) and malate (200 μM) were measured at 25ºC using a modified Clark-type O_2-electrode (Hansatech Instruments). Respiration rates are expressed as nmol O_2 consumed min^{-1} mg dry weight^{-1}. For assessment of mitochondrial content red and white vastus lateralis muscles were isolated from *mkp-1*$^{+/+}$ and *mkp-1*$^{-/-}$ mice. DNA was isolated with the DNEasy DNA isolation kit (Qiagen) and PCR was performed with the BioRad iQ5 Real-Time PCR Detection System using Sybr Green fluorophore with the following primers for: 18S – 5′-TAGAGGGACAAGTGGCGTTC-3′ and 5′-CGCTGAGCCAGTC AGTGT-3′, mouse mitochondrial Cox1 5′-GCCCCAGATATAGCATTCCC-3′ and 5′- GTTCATCCTGTTCCTGCTCC-3′. Critical thresholds of mitochondrial DNA were subtracted from the critical thresholds of nuclear DNA to obtain a ratio of mitochondrial DNA/nuclear DNA.

Luciferase reporter assays

Luciferase and Renilla activities were measured using the dual luciferase reporter assay system kit from Promega (Madison, WI) according to the manufacturer's instructions. Primary *mkp-1*$^{+/+}$ and *mkp-1*$^{-/-}$ hepatocytes were transiently transfected with 1.0 μg $(ACO)_3$-TK-Luc and 50 ng pRL-*Renilla* or 0.5 μg GAL4-c-Jun, 0.5 μg 5 x GAL4-Luciferase and 50 ng pRL-*Renilla* with lipofectamine 2000. Hepatocytes were stimulated for 5 hr with 200 μM

ciprofibrate or 200 μM ciprofibrate plus 5 μM SB203580 prior to measuring luciferase and renilla activities.

Statistical analyses

MAPK assays were quantitated using LabWorks 4.0™ densitometric software (UVP Inc., Upland, CA). Statistical significances between groups were calculated by two-way t test assuming equal variances using Microsoft Excel Statistical Analysis Tool (Microsoft, Redmond, WA). Growth curves and GTTs were analyzed by One-way ANOVA with Bonferoni post-test performed using GraphPad InStat version 3.05 for Windows 95/NT (GraphPad Software, San Diego).

Supplemental data

Supplemental data include one table and four figures and can be found with this article online at http://www.cellmetabolism.org/cgi/content/full/4/1/61/DC1/.

Acknowledgments

We thank Lei Zhang and Tim Yu for technical assistance, Katherine Augustyn and Albert Menonne (Yale Liver Center [2P30 DK34989]) for hepatocyte preparations, and Dr. Shadel for assistance with mitochondrial content experiments. We thank Dr. Daniel Kelly for providing $(ACO)_3$-TK-Luc. This work was supported by P01-DK57751 and a Liver Pilot Project grant (P30 34989) to A.M.B. and T32 CA09085 to J.J.W. J.K.K. was supported by U24-DK59635 and the American Diabetes Association (1-04-RA-47). G.I.S. was supported by R01 DK-40936 and a Distinguished Clinical Scientist Award from the American Diabetes Association.

Received: December 12, 2005
Revised: April 7, 2006
Accepted: May 18, 2006
Published: July 4, 2006

References

Aguirre, V., Uchida, T., Yenush, L., Davis, R., and White, M.F. (2000). The c-Jun NH2-terminal Kinase Promotes Insulin Resistance during Association with Insulin Receptor Substrate-1 and Phosphorylation of Ser307. J. Biol. Chem. *275*, 9047–9054.

Anderson, E.J., and Neufer, P.D. (2006). Type II skeletal myofibers possess unique properties that potentiate mitochondrial H2O2 generation. Am. J. Physiol. Cell Physiol. *290*, C844–C851.

Barger, P.M., Brandt, J.M., Leone, T.C., Weinheimer, C.J., and Kelly, D.P. (2000). Deactivation of peroxisome proliferator-activated receptor-{alpha} during cardiac hypertrophic growth. J. Clin. Invest. *105*, 1723–1730.

Barger, P.M., Browning, A.C., Garner, A.N., and Kelly, D.P. (2001). p38 mitogen-activated protein kinase activates peroxisome proliferator-activated receptor alpha: a potential role in the cardiac metabolic stress response. J. Biol. Chem. *276*, 44495–44501.

Bays, H., Mandarino, L., and DeFronzo, R.A. (2004). Role of the adipocyte, free fatty acids, and ectopic fat in pathogenesis of type 2 diabetes mellitus: peroxisomal proliferator-activated receptor agonists provide a rational therapeutic approach. J. Clin. Endocrinol. Metab. *89*, 463–478.

Bost, F., Aouadi, M., Caron, L., Even, P., Belmonte, N., Prot, M., Dani, C., Hofman, P., Pages, G., Pouyssegur, J., et al. (2005). The extracellular signal-regulated kinase isoform ERK1 is specifically required for in vitro and in vivo adipogenesis. Diabetes *54*, 402–411.

Boyer, J.L., Phillips, J.M., Graf, J., Fleischer, S., and Becca, F. (1990). Preparation and specific applications of isolated hepatocyte couplets. In Methods in Enzymology (Academic Press), pp. 501–516.

Bradley, R.L., Mansfield, J.P., Maratos-Flier, E., and Cheatham, B. (2002). Melanin-concentrating hormone activates signaling pathways in 3T3–L1 adipocytes. Am. J. Physiol. Endocrinol. Metab. *283*, E584–E592.

Brancho, D., Tanaka, N., Jaeschke, A., Ventura, J.J., Kelkar, N., Tanaka, Y., Kyuuma, M., Takeshita, T., Flavell, R.A., and Davis, R.J. (2003). Mechanism of p38 MAP kinase activation in vivo. Genes Dev. *17*, 1969–1978.

Camps, M., Nichols, A., and Arkinstall, S. (2000). Dual specificity phosphatases: a gene family for control of MAP kinase function. FASEB J. *14*, 6–16.

Cao, W., Collins, Q.F., Becker, T.C., Robidoux, J., Lupo, E.G., Jr., Xiong, Y., Daniel, K.W., Floering, L., and Collins, S. (2005). p38 Mitogen-activated Protein Kinase Plays a Stimulatory Role in Hepatic Gluconeogenesis. J. Biol. Chem. *280*, 42731–42737.

Chi, H., Barry, S.P., Roth, R.J., Wu, J.J., Jones, E.A., Bennett, A.M., and Flavell, R.A. (2006). Dynamic regulation of pro- and anti-inflammatory cytokines by MAPK phosphatase 1 (MKP-1) in innate immune responses. Proc. Natl. Acad. Sci. USA *103*, 2274–2279.

Chin, S., Ramirez, S., Greenbaum, L.E., Naji, A., and Taub, R. (1995). Blunting of the immediate-early gene and mitogenic response in hepatectomized type 1 diabetic animals. Am. J. Physiol. Endocrinol. Metab. *269*, E691–E700.

Christie, G.R., Williams, D.J., MacIsaac, F., Dickinson, R.J., Rosewell, I., and Keyse, S.M. (2005). The Dual-Specificity Protein Phosphatase DUSP9/MKP-4 Is Essential for Placental Function but Is Not Required for Normal Embryonic Development. Mol. Cell. Biol. *25*, 8323–8333.

Clapham, J.C., Arch, J.R.S., Chapman, H., Haynes, A., Lister, C., Moore, G.B.T., Piercy, V., Carter, S.A., Lehner, I., Smith, S.A., et al. (2000). Mice overexpressing human uncoupling protein-3 in skeletal muscle are hyperphagic and lean. Nature *406*, 415–418.

Davis, R.J. (2000). Signal transduction by the JNK group of MAP kinases. Cell *103*, 239–252.

Dorfman, K., Carrasco, D., Gruda, M., Ryan, C., Lira, S.A., and Bravo, R. (1996). Disruption of the *erp/mkp-1* gene does not affect mouse development: normal MAP kinase activity in ERP/MKP-1-deficient fibroblasts. Oncogene *13*, 925–931.

Esteves, T.C., and Brand, M.D. (2005). The reactions catalysed by the mitochondrial uncoupling proteins UCP2 and UCP3. Biochimica et Biophysica Acta (BBA). Bioenergetics *1709*, 35–44.

Finck, B.N., Bernal-Mizrachi, C., Han, D.H., Coleman, T., Sambandam, N., LaRiviere, L.L., Holloszy, J.O., Semenkovich, C.F., and Kelly, D.P. (2005). A potential link between muscle persoxome proliferator-activated receptor-a signaling and obesity-related diabetes. Cell Metab. *1*, 133–144.

Gum, R.J., Gaede, L.L., Heindel, M.A., Waring, J.F., Trevillyan, J.M., Zinker, B.A., Stark, M.E., Wilcox, D., Jirousek, M.R., Rondinone, C.M., and Ulrich, R.G. (2003). Antisense Protein Tyrosine Phosphatase 1B Reverses Activation of p38 Mitogen-Activated Protein Kinase in Liver of ob/ob Mice. Mol. Endocrinol. *17*, 1131–1143.

Hammer, M., Mages, J., Dietrich, H., Servatius, A., Howells, N., Cato, A.C.B., and Lang, R. (2006). Dual specificity phosphatase 1 (DUSP1) regulates a subset of LPS-induced genes and protects mice from lethal endotoxin shock. J. Exp. Med. *203*, 15–20.

Hirosumi, J., Tuncman, G., Chang, L., Gorgun, C.Z., Uysal, K.T., Maeda, K., Karin, M., and Hotamisligil, G.S. (2002). A central role for JNK in obesity and insulin resistance. Nature *420*, 333–336.

Keyse, S.M. (2000). Protein phosphatases and the regulation of mitogen-activated protein kinase signalling. Curr. Opin. Cell Biol. *12*, 186–192.

Keyse, S.M., and Emslie, E.A. (1992). Oxidative stress and heat shock induce a human gene encoding a protein-tyrosine phosphatase. Nature *359*, 644–647.

Kopelman, P.G. (2000). Obesity as a medical problem. Nature *404*, 635–643.

Lee, Y.H., Giraud, J., Davis, R.J., and White, M.F. (2003). c-Jun N-terminal kinase (JNK) mediates feedback inhibition of the insulin signaling cascade. J. Biol. Chem. *278*, 2896–2902.

Leng, Y., Steiler, T.L., and Zierath, J.R. (2004). Effects of Insulin, Contraction, and Phorbol Esters on Mitogen-Activated Protein Kinase Signaling in Skeletal Muscle From Lean and ob/ob Mice. Diabetes *53*, 1436–1444.

Li, S.Y., Liu, Y., Sigmon, V.K., McCort, A., and Ren, J. (2005). High-fat diet enhances visceral advanced glycation end products, nuclear O-Glc-Nac modification, p38 mitogen-activated protein kinase activation and apoptosis. Diabetes Obes. Metab. *7*, 448–454.

Mastaitis, J.W., Wurmbach, E., Cheng, H., Sealfon, S.C., and Mobbs, C.V. (2005). Acute induction of gene expression in brain and liver by insulin-induced hypoglycemia. Diabetes *54*, 952–958.

Mohn, K.L., Laz, T.M., Hsu, J.-C., Melby, A.E., Bravo, R., and Taub, R. (1991). The immediate-early growth response in regenerating liver and insulin- stimulated H-35 cells: comparison with serum-stimulated 3T3 cells and identification of 41 novel immediate-early genes. Mol. Cell. Bio. *11*, 381–390.

Nimah, M., Zhao, B., Denenberg, A.G., Bueno, O., Molkentin, J., Wong, H.R., and Shanley, T.P. (2005). Contribution of MKP-1 regulation of p38 to endotoxin tolerance. Shock *23*, 80–87.

Nishina, H., Vaz, C., Billia, P., Nghiem, M., Sasaki, T., De la Pompa, J.L., Furlonger, K., Paige, C., Hui, C., Fischer, K.D., et al. (1999). Defective liver formation and liver cell apoptosis in mice lacking the stress signaling kinase SEK1/MKK4. Development *126*, 505–516.

Ono, K., and Han, J. (2000). The p38 signal transduction pathway: activation and function. Cell. Signal. *12*, 1–13.

Park, S.Y., Cho, Y.R., Finck, B.N., Kim, H.J., Higashimori, T., Hong, E.G., Lee, M.K., Danton, C., Deshmukh, S., Cline, G.W., et al. (2005). Cardiac-Specific Overexpression of Peroxisome Proliferator-Activated Receptor-{alpha} Causes Insulin Resistance in Heart and Liver. Diabetes *54*, 2514–2524.

Puigserver, P., Rhee, J., Lin, J., Wu, Z., Yoon, J.C., Zhang, C.Y., Krauss, S., Mootha, V.K., Lowell, B.B., and Spiegelman, B.M. (2001). Cytokine stimulation of energy expenditure through p38 MAP kinase activation of PPARgamma coactivator-1. Mol. Cell *8*, 971–982.

Rahmouni, K., Morgan, D.A., Morgan, G.M., Liu, X., Sigmund, C.D., Mark, A.L., and Haynes, W.G. (2004). Hypothalamic PI3K and MAPK differentially mediate regional sympathetic activation to insulin. J. Clin. Invest. *114*, 652–658.

Reddy, S.T., Nguyen, J.T., Grijalva, V., Hough, G., Hama, S., Navab, M., and Fogelman, A.M. (2004). Potential role for mitogen-activated protein kinase phosphatase-1 in the development of atherosclerotic lesions in mouse models. Arterioscler. Thromb. Vasc. Biol. *24*, 1676–1681.

Rodriguez, A., Duran, A., Selloum, M., Champy, M.-F., Diez-Guerra, F.J., Flores, J.M., Serrano, M., Auwerx, J., Diaz-Meco, M.T., and Moscat, J. (2006). Mature-onset obesity and insulin resistance in mice deficient in the signaling adapter p62. Cell Metab. *3*, 211–222.

Sakaue, H., Ogawa, W., Nakamura, T., Mori, T., Nakamura, K., and Kasuga, M. (2004). Role of MAPK phosphatase-1 (MKP-1) in adipocyte differentiation. J. Biol. Chem. *279*, 39951–39957.

Salojin, K.V., Owusu, I.B., Millerchip, K.A., Potter, M., Platt, K.A., and Oravecz, T. (2006). Essential Role of MAPK Phosphatase-1 in the Negative Control of Innate Immune Responses. J. Immunol. *176*, 1899–1907.

Sarraf, P., Frederich, R.C., Turner, E.M., Ma, G., Jaskowiak, N.T., Rivet, D.J., 3rd, Flier, J.S., Lowell, B.B., Fraker, D.L., and Alexander, H.R. (1997). Multiple cytokines and acute inflammation raise mouse leptin levels: potential role in inflammatory anorexia. J. Exp. Med. *185*, 171–175.

Shen, Y.H., Godlewski, J., Zhu, J., Sathyanarayana, P., Leaner, V., Birrer, M.J., Rana, A., and Tzivion, G. (2003). Cross-talk between JNK/SAPK and ERK/MAPK pathways: sustained activation of JNK blocks ERK activation by mitogenic factors. J. Biol. Chem. *278*, 26715–26721.

Tata, J.R., Fleischer, S., and Lester, P. (1974). Isolation of nuclei from liver and other tissues. In Methods in Enzymology (Academic Press), pp. 253–262.

Tournier, C., Whitmarsh, A.J., Cavanagh, J., Barrett, T., and Davis, R.J. (1999). The MKK7 gene encodes a group of c-Jun NH2-terminal kinase kinases. Mol. Cell. Biol. *19*, 1569–1581.

Vega, R.B., Huss, J.M., and Kelly, D.P. (2000). The coactivator PGC-1 cooperates with peroxisome proliferator-activated receptor alpha in transcriptional control of nuclear genes encoding mitochondrial fatty acid oxidation enzymes. Mol. Cell. Biol. *20*, 1868–1876.

Volmat, V., Camps, M., Arkinstall, S., Pouyssegur, J., and Lenormand, P. (2001). The nucleus, a site for signal termination by sequestration and inactivation of p42/p44 MAP kinases. J. Cell Sci. *114*, 3433–3443.

Wu, J.J., and Bennett, A.M. (2005). Essential Role for Mitogen-activated Protein (MAP) Kinase Phosphatase-1 in Stress-responsive MAP Kinase and Cell Survival Signaling. J. Biol. Chem. *280*, 16461–16466.

Wu, J.J., Zhang, L., and Bennett, A.M. (2005). The noncatalytic amino terminus of mitogen-activated protein kinase phosphatase 1 directs nuclear targeting and serum response element transcriptional regulation. Mol. Cell. Biol. *25*, 4792–4803.

Zhang, H., Shi, X., Hampong, M., Blanis, L., and Pelech, S. (2001). Stress-induced inhibition of ERK1 and ERK2 by direct interaction with p38 MAP kinase. J. Biol. Chem. *276*, 6905–6908.

Zhang, Y., Blattman, J.N., Kennedy, N.J., Duong, J., Nguyen, T., Wang, Y., Davis, R.J., Greenberg, P.D., Flavell, R.A., and Dong, C. (2004). Regulation of innate and adaptive immune responses by MAP kinase phosphatase 5. Nature *430*, 793–797.

Zhao, Q., Shepherd, E.G., Manson, M.E., Nelin, L.D., Sorokin, A., and Liu, Y. (2004). The role of mitogen-activated protein kinase phosphatase-1 in the response of alveolar macrophages to lipopolysaccharide: Attenuation of proinflammatory cytokine biosynthesis via feedback control of p38. J. Biol. Chem. *280*, 8101–8108.

Zhao, Q., Wang, X., Nelin, L.D., Yao, Y., Matta, R., Manson, M.E., Baliga, R.S., Meng, X., Smith, C.V., Bauer, J.A., et al. (2006). MAP kinase phosphatase 1 controls innate immune responses and suppresses endotoxic shock. J. Exp. Med. *203*, 131–140.